Hindawi
Complexity
Volume 2021, Article ID 5592024, 20 pages
https://doi.org/10.1155/2021/5592024

Research Article

MHD Mixed Convection Nanofluid Flow over Convectively Heated Nonlinear due to an Extending Surface with Soret Effect

Jamel Bouslimi,[1] M. A. Abdelhafez,[2] A. M. Abd-Alla,[2] S. M. Abo-Dahab,[3,4] and K. H. Mahmoud[5]

[1]*Department of Physics, College of Science, Taif University, P. O. Box 11099, Taif 21944, Saudi Arabia*
[2]*Department of Mathematics, Faculty of Science, Sohag University, Sohag 82524, Egypt*
[3]*Department of Mathematics, Faculty of Science, South Valley University, Qena 83523, Egypt*
[4]*Department of Computer Science, Faculty of Computers and Information, Luxor University, Egypt*
[5]*Department of Physics, College of Khurma University College, Taif University, P. O. Box 11099, Taif 21944, Saudi Arabia*

Correspondence should be addressed to M. A. Abdelhafez; mostafa.abdallah@yahoo.com

Received 15 February 2021; Revised 15 March 2021; Accepted 12 April 2021; Published 28 April 2021

Academic Editor: Abdel-Haleem Abdel-Aty

The aim of this paper is to investigate the flow of MHD mixed convection nanofluid flow under nonlinear heated due to an extending surface. The transfer of heat in nanofluid subject to a magnetic field and boundary conditions of convective is studied to obtain the physical meaning of the convection phenomenon. The governing partial differential equations (PDEs) of the boundary layer are reduced to ordinary differential equations (ODEs) considering a technique of the transformation of similarity. The transformed equations are solved numerically considering the technique of an efficient numerical shooting applying the Runge–Kutta technique scheme from the fourth-fifth order. The results corresponding to the dimensionless speed, temperature, concentration profiles, and the Nusselt number reduced, and the Sherwood numbers are presented by figures to display the physical meaning of the phenomena. A comparison has been made between the obtained results with the previous results obtained by others and agrees with them if the new parameters vanish. The results obtained indicate the impacts of the nondimensional governing parameters, namely, magnetic field parameter M, Soret number Sr, heat source λ, thermal buoyancy parameterλ_T , and solutal buoyancy parameterλ_C on the flow, temperature, and concentration profiles being discussed and presented graphically.

1. Introduction

Nanofluids are suspended particles of the fluid. They have particles with a nanometer size, and they have a less uniform dispersion in the rigid particles. Nanofluids have crucial usages in science and technology, marine engineering, and applications in the field of industry such as plastic, polymer industries, cancer home therapy, and building sciences. They flow through transferring vertical plane plate also having enormous applications in the field of aerosols engineering, aerodynamics, and civil engineering and because of this reason, the researchers are likely to investigate this field. Nonlinear warm air radiation and chemical reaction effects on MHD 3D Casson fluid movement in the porous medium were considered by Sulochana et al. [1]. Wahiduzzaman et al. [2] investigated MHD Casson fluid movement going through a nonisothermal porous linearly stretching sheet. Ramreddy et al. [3] analyzed the Soret effect on mixed convection flow in a nanofluid under convective boundary condition radiation and the Soret effects of MHD nanofluid moving freely from a moving vertical moving plate in the porous medium were discussed by Raju et al. [4]. The mixed convective flow of Maxwell nanofluid goes beyond an absorbent vertical stretched surface. An optimal solution is considered by Ramzan et al. [5]. Stagnation electrical MHD nanofluid varied convection with slip boundary on a stretching sheet was discussed by Hsiao [6]. Rafique et al. [7] have obtained the numerical solution of casson nanofluid streams over a nonlinear sloping surface through Soret and Dufour effects by the Keller–Box method. Mkhatshwa et al. [8] investigated the MHD mixed convective nanofluid flow about a vertical thin cylinder using the interfering

multidomain spectral collocation approach. Huang [9] analyzed the effect of non-Darcy and MHD on free convection of non-Newtonian fluids over a vertical plate which can be infiltrated in a pored medium with Soret/Dufour effects and thermal radiation.

Mahanthesh et al. [10] expanded this work by considering nonlinear radiative heat transfer in MHD three-dimensional water stream based nanofluid above a nonlinearly stretching sheet with convective boundary condition. Sivaraj and Sheremet [11] investigated the MHD accepted convection and entropy generation of ferrofluids in a void with a nonuniformly heated horizontal plate. Abad et al. [12] discussed the analysis of transfers in a reaction to the flow of hybrid nanofluid around the body discussed a trick embedded in porous media using a synthetic neural network and a special swarm improvement. Siavashi [13] studied the nanofluid and porous fins influence on natural thermal convection and entropy generation of flow within a cavity. Bilal [14] discussed the partial flow of EMHD nanoparticles with nonlight thermal radiation and sliding effects. Alomar [15] studied the analysis of the effects of unbalanced and nonbloody heat flow on natural load in a square enclosure with a hot plate in L shape. Dogonchi and Hashim [16] investigated the transfer of heat through a natural load Fe304-water nanofluid to neutralize between a wavelength circular cylinder and a rhombus cylinder. Hsiao analyzed the micropolar nanoparticle flow containing MHD and Mercury dissipation effects towards an extended sheet with a multimedia feature [17]. Dinarv et al. [18] studied Buongiorno's model for the double flux slump point of a nanofluid effect of the binary base. Kefayati and Tang [19] studied the MHD mixed convection of viscoplastic fluids in different aspect rates of a lid-driven cavity using LBM. Ramzan et al. [20] discussed the mixed flux of second grade nanofluid with lipid boundary conditions: an optimal solution. Kumar et al. [21] studied Bejan's heat and mass lines ideation of multiforce influence on convection in a pored enclosure. Aurangzaib et al. [22] investigated the influence of a fractional slide on an unstable MHD mixed convection stagnation-point flow of a micropolar fluid towards a porous contraction plate. Krishna and Chamkha [23] considered the hall and ionic slide effects on the rotation flow of MHD of the water flow of the coherent fluid through the porous medium. Zaidi and Mohyud-Din [24] are the founders of the analysis of wall jet flow for Soret, Dufour, and chemical response effects in the presence of MHD with uniform suction/injection. Machireddy and Naramgari [25] examined the heat and mass transfers in radiative MHD Carreau fluid by cross-diffusion. Alsabery et al. [26] examined the fluid structure reaction in natural load heat transfer in an implicit space with a flexible oscillating fin and partial heating. Maleki et al. [27] presented the investigation of the heat transfer and nanofluid flow over a pored plate with radiation and slip boundary conditions. Do et al. [28] studied the case of Navier when slipping at the time Darcy–Forchheimer nanofluid relies on using a spectral relaxation method. Beg [29] discussed the mixed radioactive dual magnetic flow of acid with traces of the number of Biot and Richardson's effects. Srinivasacharya and Jagadeeshwar [30] investigated the seismic flow on a porous leaf extending significantly with acidic thermal boundary conditions.

Chemi et al. [31] researched the critical impedance load of double-wall carbon nanotubes using nonlocal theoretical elasticity. Timesli [32] studied the twisting analysis of double-wall carbon nanotubes embedded in a flexible Kerr medium under axial pressure using the nonlocal Donnell shell theory. Mirjavadi et al. [33] studied the analysis of fine nonlinear forced vibrations of two-phase magnetic flexible nanoparticles under elliptical type force. Some related investigations can be found in the article [34].

In this investigation, the researchers aim at presenting the influence of the prominent Soret impact on mixed convection heat and mass transfer in the border layer region of a semi-infinite vertical flat plate in a nanofluid, under the circulatory motion of the boundary conditions. The consequences of nondimensional governing parameters, namely, the volume fraction of nanoparticles, magnetic field parameter, radiation parameter, Soret number, buoyancy parameter, and porosity parameter on the flow, temperature, and concentration profiles are discussed and presented graphically. Also, the friction aspect and Nusselt and Sherwood numbers are deliberated and demonstrated in tabular form for two nanofluids separately. Some new contributions near to the present article are discussed in [35]–[44].

2. Construction of the Problem

Let us consider two-dimensional constant MHD nanofluid flows in the region $(y > 0)$ along nonlinearly stretched sheet assuming Cartesian coordinates (x, y) chosen in which $x-$axis is measured along with the sheet whereas is $y-$axis normal to it under the influence of heat absorption/generation, magnetic field, suction, and injection parameters. The stretched sheet is assumed to have general power-law surface velocity distribution $u_w(x) = ax^n$ where $a > 0$, $n \geq 0$ are constants. We consider that the flow is concerned with a variable magnetic field of strength$B(x) = B_0 x^{(n-1)/2}$. The induced magnetic field is neglected whereas the electric field is absent by assuming the low magnetic Reynolds number. The temperature of the sheet is defined by a function $T_w(x) = T_\infty + Ax^n$ where $A > 0$ is constant, T_∞ is the ambient fluid temperature, and C_∞ is the ambient nanoparticles concentration. The coordinate system and physical flow are shown in Figure 1.

The equation of rheological state for the anisotropic flow of a Casson fluid [1, 2]:

$$\tau_{ij} = \begin{cases} 2\left(\mu_B + \dfrac{P_z}{\sqrt{2\pi}}\right)e_{ij}, & \pi > \pi_c, \\ \\ 2\left(\mu_B + \dfrac{P_z}{\sqrt{2\pi}}\right)e_{ij}, & \pi < \pi_c, \end{cases} \tag{1}$$

where $\pi = e_{ij}e_{ij}$,

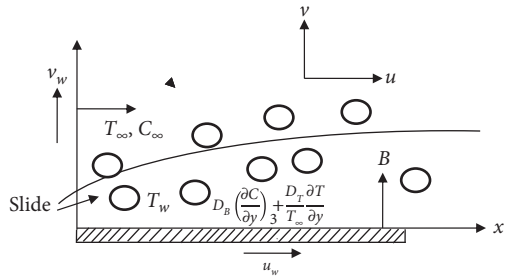

Figure 1: Diagrammatic of the problem.

$$\frac{\partial u}{\partial x}+\frac{\partial v}{\partial y}=0, \tag{2}$$

$$u\frac{\partial u}{\partial x}+v\frac{\partial u}{\partial y}=v\left(1+\frac{1}{\beta}\right)\left(\frac{\partial^2 u}{\partial y^2}\right)+g\left[\alpha_T\left(T-T_\infty\right)+\alpha_C\left(C-C_\infty\right)\right]-\frac{\sigma B^2(x)}{\rho_f}u, \tag{3}$$

$$u\frac{\partial T}{\partial x}+v\frac{\partial T}{\partial y}=\alpha\left(\frac{\partial^2 T}{\partial y^2}\right)+\frac{Q_0}{\rho c_p}\left(T-T_\infty\right)+\tau\left[D_B\left(\frac{\partial T}{\partial y}\frac{\partial C}{\partial y}\right)+\frac{D_T}{T_\infty}\left(\frac{\partial T}{\partial y}\right)^2\right]+\frac{\nu}{c_p}\left(1+\frac{1}{\beta}\right)\left(\frac{\partial u}{\partial y}\right)^2, \tag{4}$$

$$u\frac{\partial C}{\partial x}+v\frac{\partial C}{\partial y}=D_B\left(\frac{\partial^2 C}{\partial y^2}\right)+\frac{K_T D_T}{T_\infty}\left(\frac{\partial^2 T}{\partial y^2}\right), \tag{5}$$

where u and v are the velocity components along the $x-$ and $y-$directions respectively, υ is the kinematic viscosity, $\beta=\mu_B\sqrt{2\pi_c}/P_y$ is Casson fluid parameter,σ is the electrical conductivity, ρ is the fluid density, the thermal diffusivity is denoted by α, D_B and D_T are the coefficients of the thermophoresis and Brownian diffusions, Q_0 is the dimensional heat generation or absorption coefficient, c_p is the specific heat, $\tau=(\rho c)_p/(\rho c)_f$ indicates the ratio of effective heat capacity of the nanoparticle material to the effective heat capacity of the fluid, g is the acceleration due to gravity, α_T is the thermal expansion coefficient, α_C is the concentration expansion coefficient, and K_T is the thermal diffusion ratio. The boundary conditions in the present problem are

$$\begin{cases} u=u_w(x)=ax^n, v=v_w, T=T_w(x)=T_\infty+Ax^n, D_B\left(\frac{\partial C}{\partial y}\right)+\frac{D_T}{T_\infty}\frac{\partial T}{\partial y} \text{ at } y=0, \\ u\longrightarrow 0, T\longrightarrow T_\infty, C\longrightarrow C_\infty \text{ as } y\longrightarrow\infty. \end{cases} \tag{6}$$

The nondimensional transformations are taken as follows:

$$\begin{cases} u=ax^n f'(\eta), v=-ax^{(n-1)/2}\sqrt{\frac{v}{a}}\left(\frac{n+1}{2}f(\eta)+\frac{n-1}{2}\eta f'(\eta)\right), \quad \eta=\sqrt{\frac{a}{v}}x^{(n-1)/2}y, \\ \theta(\eta)=\frac{T-T_\infty}{T_w-T_\infty}, \qquad\qquad \phi(\eta)=\frac{C-C_\infty}{C_w-C_\infty}, \end{cases} \tag{7}$$

$$\left(1+\frac{1}{\beta}\right)f'''(\eta)-nf'^2(\eta)+\frac{n+1}{2}f(\eta)f''(\eta)-Mf'(\eta)+\lambda_T\theta+\lambda_C\phi=0, \tag{8}$$

$$\frac{1}{\mathrm{Pr}}\theta''+\frac{n+1}{2}f\theta'-nf'\theta+\lambda\theta+\mathrm{Nb}\theta'\phi'+\mathrm{Nt}\theta'^2+\left(1+\frac{1}{\beta}\right)\mathrm{Ec}f''^2=0, \tag{9}$$

$$\varphi''+\frac{n+1}{2}\mathrm{Le}f\phi'+\mathrm{LeSr}\theta''=0. \tag{10}$$

The boundary conditions are

$$\left.\begin{aligned} &f(0) = f_w, f'(0) = 1, \theta(0) = 1, \mathrm{Nb}\phi'(0) + \mathrm{Nt}\theta'(0) = 0, && \text{at } \eta = 0, \\ &f'(\infty) \longrightarrow 0, \theta(\infty) \longrightarrow 0, \phi(\infty) \longrightarrow 0, && \text{as } \eta \longrightarrow \infty, \end{aligned}\right\}, \tag{11}$$

where Ec is Eckert number, $f_w$is absorption/intromission variable ($f_w > 0$) for absorption and ($f_w < 0$) for intromission), M is the attractive field variable, Nb is the Brownian motion variable, Nt is the thermophoresis parameter, Pr is the Prandtl number, Le is the Lewis number, λ is the birthplace of heat ($\lambda > 0$) or sink parameter ($\lambda < 0$), Sr is Soret number, λ_T is thermal buoyancy parameter, and λ_C is solutal buoyancy variable. These are specified as follows:

$$\begin{aligned} M &= \frac{\sigma B^2}{a x^{n-1} \rho_f}, \\ K &= \frac{\upsilon}{a x^{n-1} k}, \\ \lambda_T &= \frac{\mathrm{Gr}_x}{\mathrm{Re}_x} = \frac{\alpha_T g}{a^2 x^{n-1} x^n} (T_w - T_\infty), \\ \lambda_C &= \frac{\mathrm{Gc}_x}{\mathrm{Re}_x} = \frac{\alpha_C g}{a^2 x^{n-1} x^n} (C_w - C_\infty), \\ \mathrm{Gr}_x &= \frac{\alpha_T g (T_w - T_\infty) x^3}{\upsilon^2}, \\ \mathrm{Gc}_x &= \frac{\alpha_C g (C_w - C_\infty) x^3}{\upsilon^2}, \\ \mathrm{Re}_x &= \frac{u_w(x) x}{\upsilon} = \frac{a x^{n+1}}{\upsilon}, \\ \mathrm{Pr} &= \frac{\upsilon}{\alpha}, \\ \lambda &= \frac{Q_0}{\rho c_p}, \\ \mathrm{Nb} &= \tau \frac{D_B (C_w - C_\infty)}{\upsilon}, \\ \mathrm{Nt} &= \tau \frac{D_T (T_w - T_\infty)}{T_\infty \upsilon}, \\ \mathrm{Ec} &= \frac{u_w^2}{(T_w - T_\infty) c_p}, \\ \mathrm{Le} &= \frac{\upsilon}{D_B}, \\ \mathrm{Sr} &= \left(\frac{K_T D_T (T_w - T_\infty)}{\upsilon T_\infty (C_w - C_\infty)} \right). \end{aligned} \tag{12}$$

The amounts of practical interest include the coefficient of skin abrasion C_f, regional Nusselt volume Nu_x, and local Sherwood volume Sh_x specified as follows:

$$\begin{aligned} C_{fx} &= \frac{\tau_w}{\rho u_w^2}, \\ \mathrm{Nu}_x &= \frac{x q_w}{\alpha (T_w - T_\infty)}, \\ \mathrm{Sh}_x &= \frac{x q_m}{D_B (C_w - C_\infty)}, \end{aligned} \tag{13}$$

where τ_w is the stress of wall clipping; α_f is the thermal conductivity of the nanofluid; and q_w, q_m are the wall heat and mass influx. These are given by

$$\begin{aligned} \tau_w &= \mu_B \left(1 + \frac{1}{\beta}\right) \left(\frac{\partial u}{\partial y}\right)_{y=0}, \\ q_w &= -\alpha_f \left(\frac{\partial T}{\partial y}\right)_{y=0}, \\ q_m &= -D_B \left(\frac{\partial C}{\partial y}\right)_{y=0}. \end{aligned} \tag{14}$$

Using equations (7) and (14) in equation (13), one obtains

$$\begin{aligned} \mathrm{Re}_x^{1/2} C_{fx} &= \left(1 + \frac{1}{\beta}\right) f'(0), \\ \mathrm{Re}_x^{-1/2} \mathrm{Nu}_x &= -\theta'(0), \\ \mathrm{Re}_x^{-1/2} \mathrm{Sh}_x &= -\phi'(0), \end{aligned} \tag{15}$$

where $\mathrm{Re}_x = u_w x/\upsilon$ is the local Reynolds number.

3. Numerical Results and Discussion

The orders of not linear normal distinctive equation (3) for (5) with the limit situation (6) are detached in terms of numbers by the Rung–Kutta method with MATLAB package. The outcome displays show the influences of the nondimensional controlling variable, which is magnetic area variable M, Soret number Sr, birthplace of heat λ, thermic buoyancy parameter λ_T, and solutal buoyancy parameter λ_C on the flow, heat, and concentricity profiles are shown and illustrated diagrammatically. The agent of rubbing and Nusselt and Sherwood numbers is discussed and given in tabular form for two nanofluids individually. The numeral outcomes are as follows:

$$\begin{aligned} \mathrm{Pr} &= 0.7, \\ \mathrm{Le} &= 0.4, \\ \mathrm{Nb} = \mathrm{Nt} &= 0.3, \\ \mathrm{Ec} &= 0.5, \\ \lambda &= 0.1, \\ \beta &= 0.5, \\ \mathrm{Fw} &= 0.2, \\ n &= 2. \end{aligned} \tag{16}$$

Figures 2–4 show that the difference of speed $f'(\eta)$, heat $\theta(\eta)$, and concentricity $\phi(\eta)$ with respect to η -axis for various amounts of λ_C. There is an observation of the velocity decrease along with the increase of λ_C, whereas there is an increase of both the heat and concentricity profiles along with the increase of λ_C for magnetic field parameter $M = 1, 2$. This causes development in both the thermic stretched sheet thickness and velocity and concentration sheet thickness. From these figures, it is observed that the increase of magnetic area parameter leads to the increase of velocity. It is also interesting to note from Figure 3 that temperature rises as M increases; Figure 4 also shows the fall of concentricity while the magnetic area parameter increases.

Figures 5–7 display variance of speed $f'(\eta)$, heat $\theta(\eta)$, and concentration $\phi(\eta)$ with respect to η-axis for various amounts of thermic buoyancy parameter λ_T. The increase of velocity along with the increase of thermic buoyancy parameter λ_T is noticed, whereas the heat and centricity profiles reduce with the growing flux of magnetic area parameter. This causes development in both the thermic stretched sheet thickness and velocity and concentration sheet thickness.

Figures 8–10 show the alteration velocity $f'(\eta)$, temperature $\theta(\eta)$, and concentricity $\phi(\eta)$ with respect to η-axis for various numbers of thermal buoyancy parameter λ_T. It is noticed that the velocity value increases along with thermal buoyancy parameter λ_T, whereas the temperature and the concentricity profiles fall with the increase of thermal buoyancy parameter λ_T of the flux for the Solutal buoyancy parameter$\lambda_C = 0.5, 1$. This causes to make the thickness of both the thermic stretched sheet and velocity and concentricity sheet better.

Figures 11–13 plot the velocity variance $f'(\eta)$, temperature $\theta(\eta)$, and concentration $\phi(\eta)$ with respect to η-axis for various numbers of magnetic area parameter M. It is watched that, by the growing of magnetic area parameter, the velocity value grows too. However, the increase of the magnetic field area causes a reduction in the profiles of temperature and concentricity. This leads to developing the thermic stretched sheet thickness along with velocity and concentration sheet thickness.

Figures 14–16 clear the different values of velocity $f'(\eta)$, temperature $\theta(\eta)$, and concentration $\phi(\eta)$ with respect to η-axis for changeable values of magnetic field parameter. By observation, it is clear that the increasing positive values of the magnetic area cause the reduction of velocity which also grows along with the reduction of negative values of a magnetic area, while it increases with decreasing of negative values of the magnetic field, though the temperature increases with decreasing the negative values of the magnetic field. Also, there is no effect of the positive values of magnetic field on the temperature, and the concentration outlines increase with increasing the negative values of the magnetic field parameter, while as well it is not affected by positive values of magnetic field on the concentration. This causes thermal stretched sheet thickness to get better along with velocity and concentration sheet thickness.

Figures 17–19 illustrate the difference of velocity $f'(\eta)$, temperature $\theta(\eta)$, and concentricity $\phi(\eta)$ with respect to η-axis for different values of Soret number Sr. The growth of profiles of both the velocity and concentricity is noted along with the increase of Soret number for $n = 0.5, 2$, while the temperature profiles go down with the increase of Soret number of the flow for $n = 0.5, 2$. This leads to making the thermal stretched sheet thickness better along with velocity and concentration sheet thickness.

Figures 20–22 show the variance of velocity $f'(\eta)$, temperature $\theta(\eta)$, and concentricity $\phi(\eta)$ with respect to η-axis for different values of Soret number Sr. It is watched that the increasing Soret number causes the increase of velocity and the decrease of temperature; however, both of them are not affected by Lewis number Le on the velocity and temperature, while the concentration profiles increase with increasing Soret number of the flow, but they are not affected by Lewis number on the concentration. These causes developing the thermal stretched sheet thickness along with velocity and concentration sheet thickness.

Figure 23 plots the diversity of Nusselt number $\mathrm{Nu}_x\mathrm{Re}_x^{1/2}$ with respect to Solutal buoyancy parameter λ_C-axis for various numbers of thermal buoyancy parameter λ_T and magnetic field M. Through observation, it is clear that the Nusselt number grows up along with the increasing thermic buoyancy parameter but falls with the increasing magnetic area.

Figure 24 displays the difference of the Nusselt number $\mathrm{Nu}_x\mathrm{Re}_x^{1/2}$ with respect to Lewis number Le-axis for different values of Soret number Sr and thermal buoyancy parameter λ_T. It is noticed that the increase of both the Sort number and thermic buoyancy parameter causes the Nusselt number to increase as well.

Figure 25 clears the variance of the Nusselt number $\mathrm{Nu}_x\mathrm{Re}_x^{-1/2}$ with respect to λ_c-axis for different values of the Soret number Sr and thermal buoyancy parameter λ_T. There is a notice that the Nusselt number grows along with the increase of both the Soret number and thermic buoyancy parameter.

Figure 26 shows the variation of the Sherwood number $\mathrm{Sh}_x(\mathrm{Re}_x)^{-1/2}$ with respect to solutal buoyancy parameter λ_C-axis for various numbers of thermal buoyancy parameter λ_T and magnetic field M. It is clear that the Sherwood number goes up with the progress of the thermic buoyancy parameter but it goes down with the progress of the magnetic field.

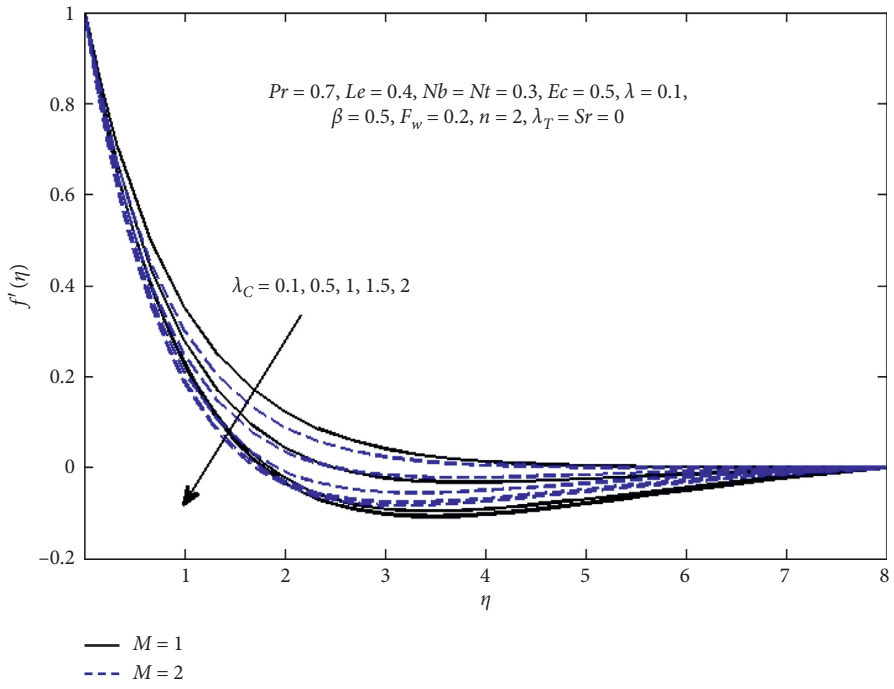

Figure 2: Variation of velocity f' concerning η with various values of λ_c ($M = 1$——, $M = 2$ ---).

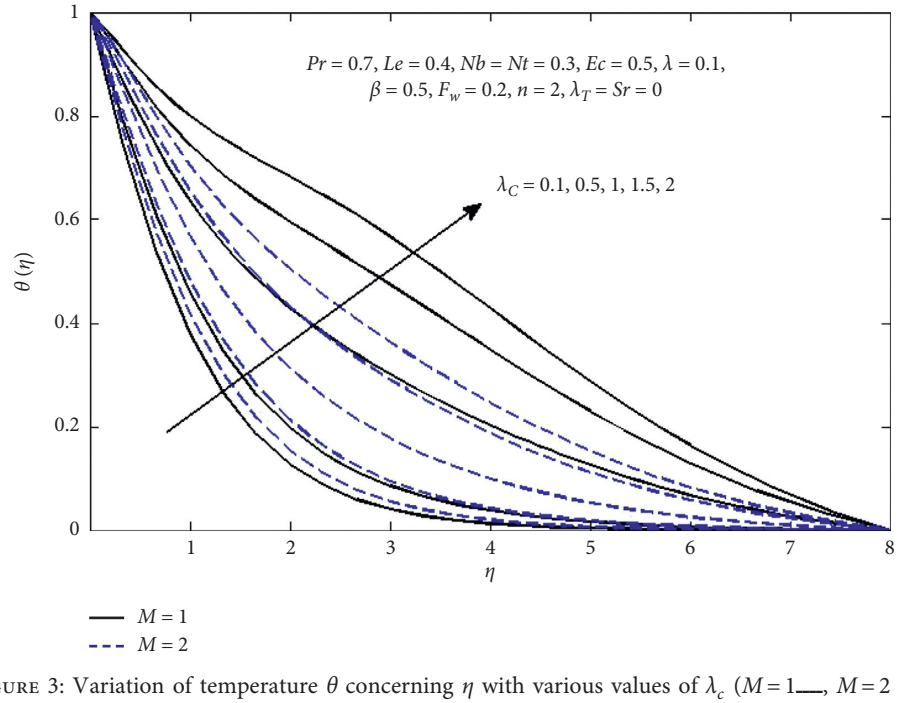

Figure 3: Variation of temperature θ concerning η with various values of λ_c ($M = 1$——, $M = 2$ ---).

Table 1 displays a comparison for the heat transfer rate at the sheet for different values of n, β, and M, when $\mathrm{Ec} = f_w = \lambda = 0, \mathrm{Nt} = \mathrm{Nb} = 0.5, \mathrm{Pr} = 7$. It is strongly obvious that the present study has original values near the results obtained by the others [9].

Table 2 shows the heat transfer rate at the sheet for numerous values of $\mathrm{Sr}, \lambda_T, \lambda_C, \beta, f_w$, and M when $\mathrm{Nt} = \mathrm{Nb} = 0.5, \mathrm{Pr} = 7, n = 1, \mathrm{Ec} = 0.5$. It is clear that the external parameters impact the heat transfer rate comparing with the consequences obtained in the previous works.

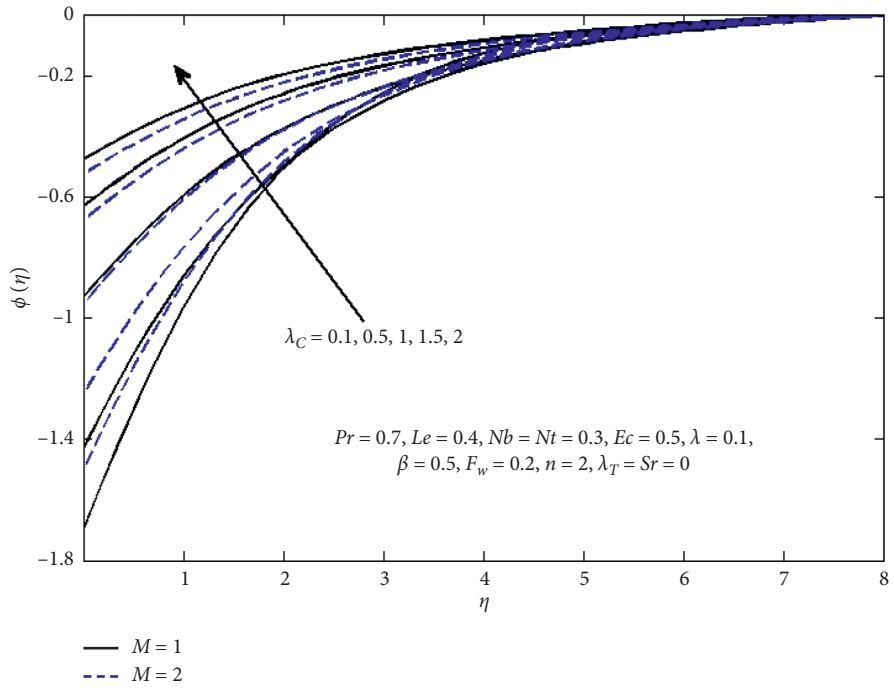

Figure 4: Variation concentration ϕ concerning η with various values of λ_c ($M = 1$——, $M = 2$ ---).

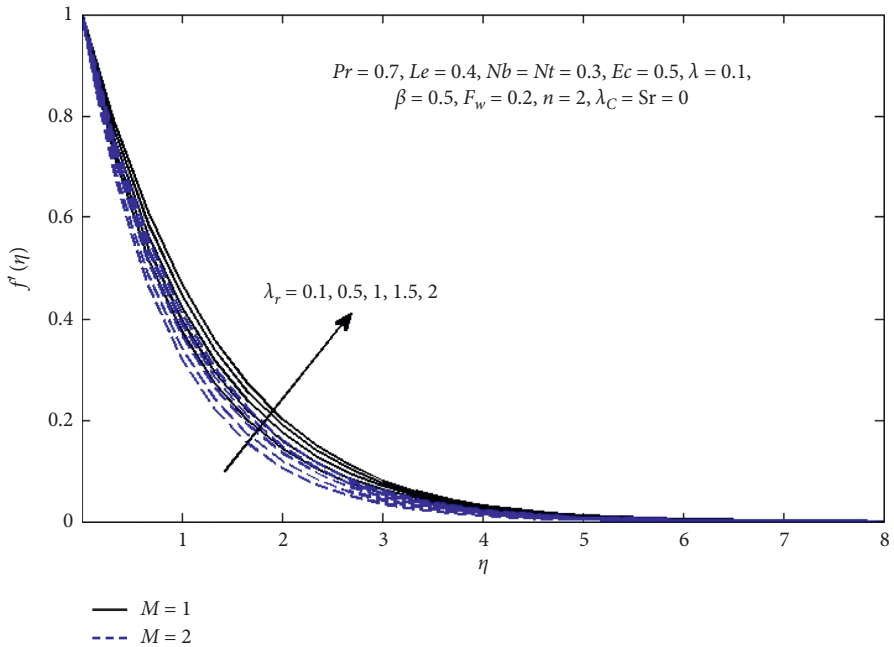

Figure 5: Variation of velocity f' concerning η with various values of λ_T ($M = 1$——, $M = 2$ ---).

Table 1: Heat transfer rate at the sheet for numerous values of n, β, and M, when Ec = $f_w = \lambda = 0$, Nt = Nb = 0.5, Pr = 7.

Constants			Ref. [9]	Present work
n	β	M	$-\theta'(0)$	$-\theta'(0)$
1	0.6	3	2.69156	2.69158
1	0.6	3	2.51354	2.51355
1	0.6	3	2.31554	2.31559
2	0.2	3	3.41143	3.41132
2	0.6	3	3.31040	3.31030
2	1.0	3	3.26319	3.26311
3	0.6	0	4.18830	4.18829
3	0.6	1	4.14820	4.14822
3	0.6	3	4.08219	4.08222

Table 2: Heat transfer rate at the sheet for numerous values of Sr, $\lambda_T, \lambda_C, \beta, f_w$, and M when Nt = Nb = 0.5, Pr = 7, n = 1, Ec = 0.5.

λ_T	λ_C	Sr	M	β	f_w	$-\theta'(0)$
0.1	0.1	0.2	3	0.6	0.2	0.11049
0.2						0.04439
	0.2					0.09518
	0.4					0.06495
		0.1				0.26966
		0.3				0.00326
0.1			1			1.33869
	0.1		2			0.58871
		0.2		0.2		0.59467
			3	0.4		0.26645
				0.6	−0.4	0.36649
					0.4	0.13465

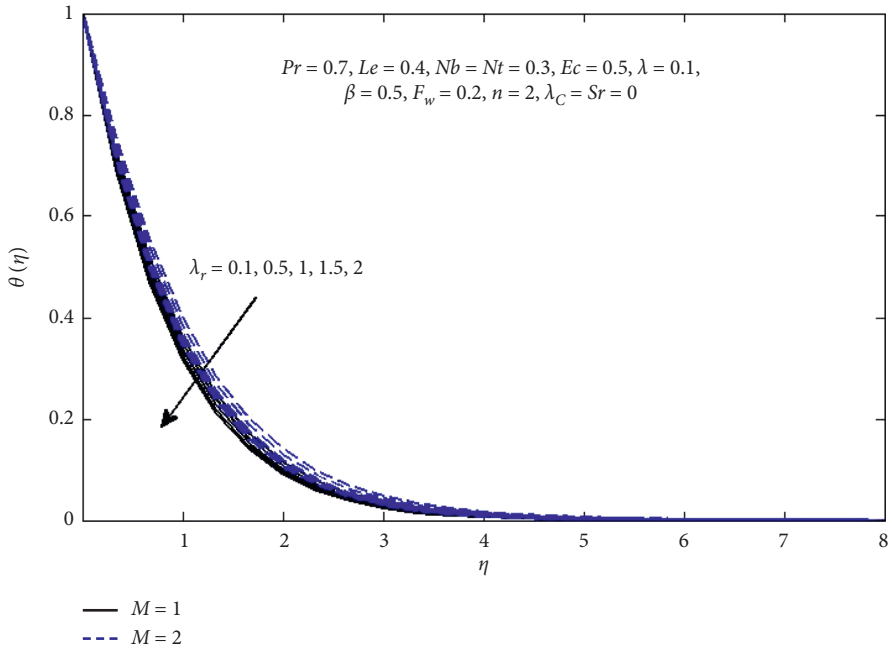

Figure 6: Variation of temperature θ concerning η with various values of λ_T ($M = 1$ ——, $M = 2$ ---).

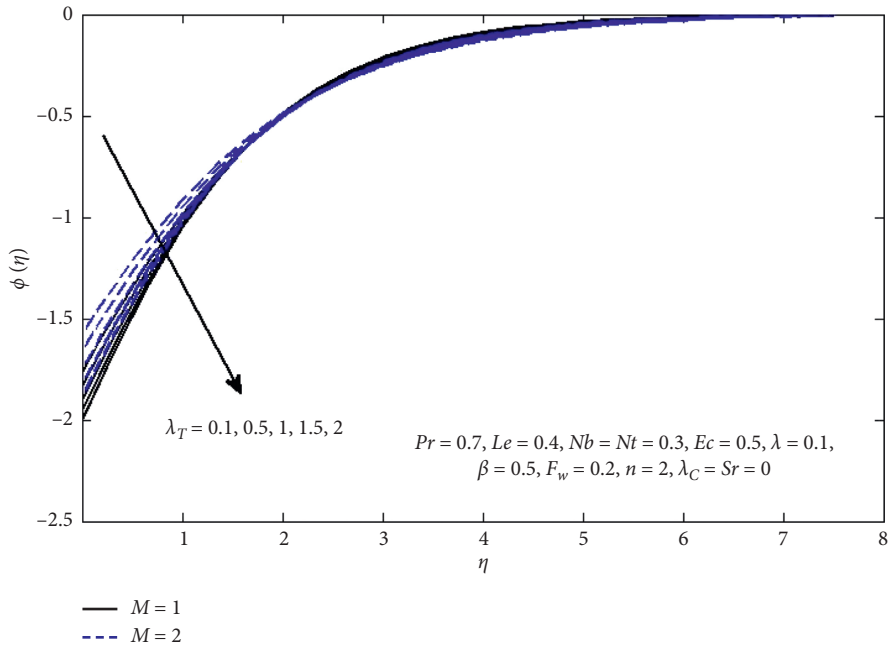

Figure 7: Distinction of concentration ϕ concerning η with various values of λ_T ($M = 1$——, $M = 2$ ---).

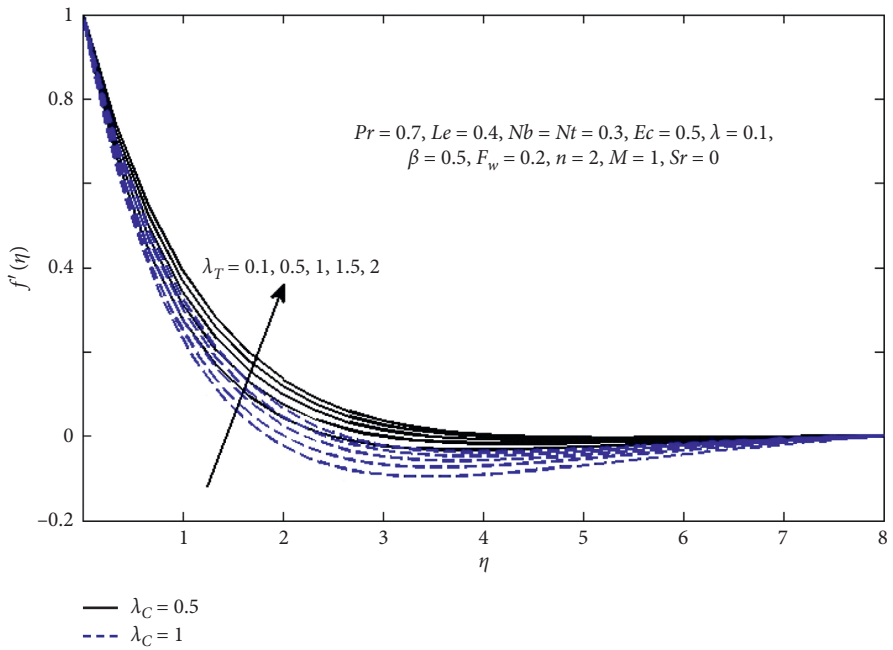

Figure 8: Diversity of velocity f' concerning η with various values of λ_T ($\lambda_c = 0.5$——, $\lambda_c = 1$---).

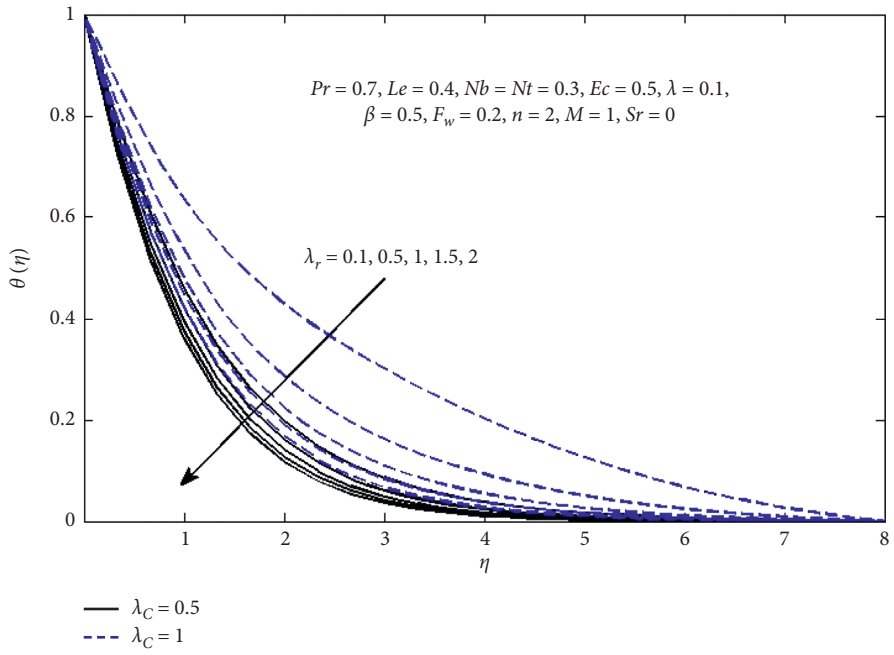

Figure 9: Variation of temperature θ concerning η with various values of λ_T ($\lambda_c = 0.5$——, $\lambda_c = 1$---).

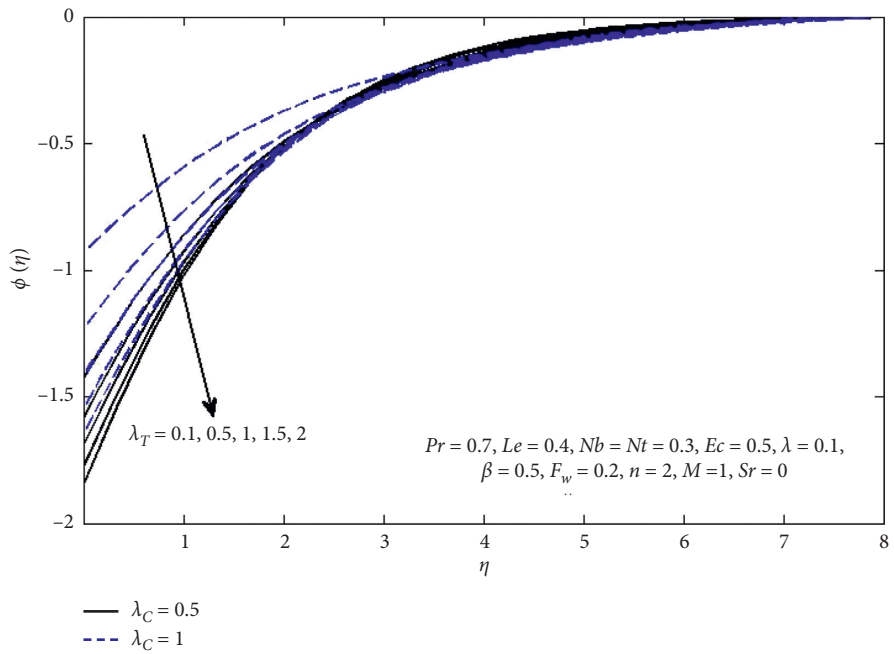

Figure 10: Variation of concentration ϕ concerning η with various values of λ_T ($\lambda_c = 0.5$——, $\lambda_c = 1$---).

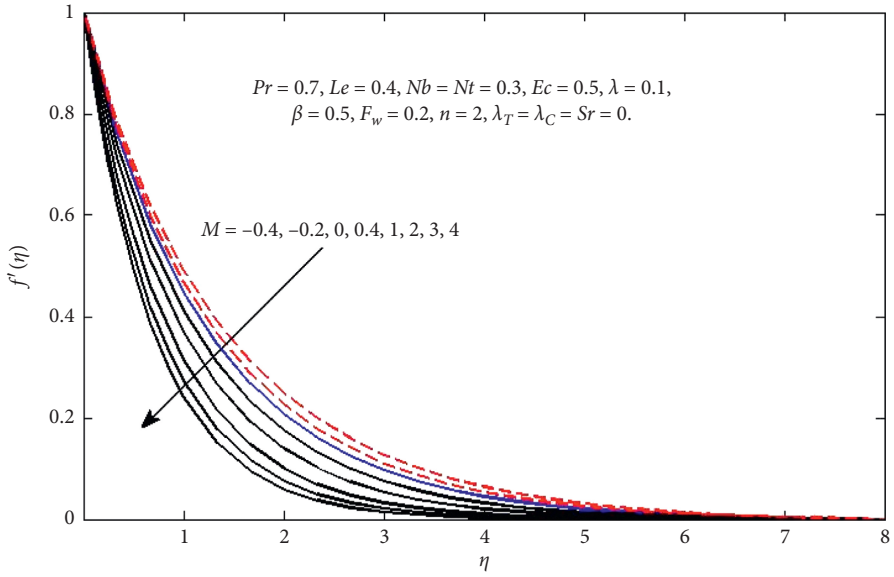

Figure 11: Variation of velocity f' concerning η with various values of M.

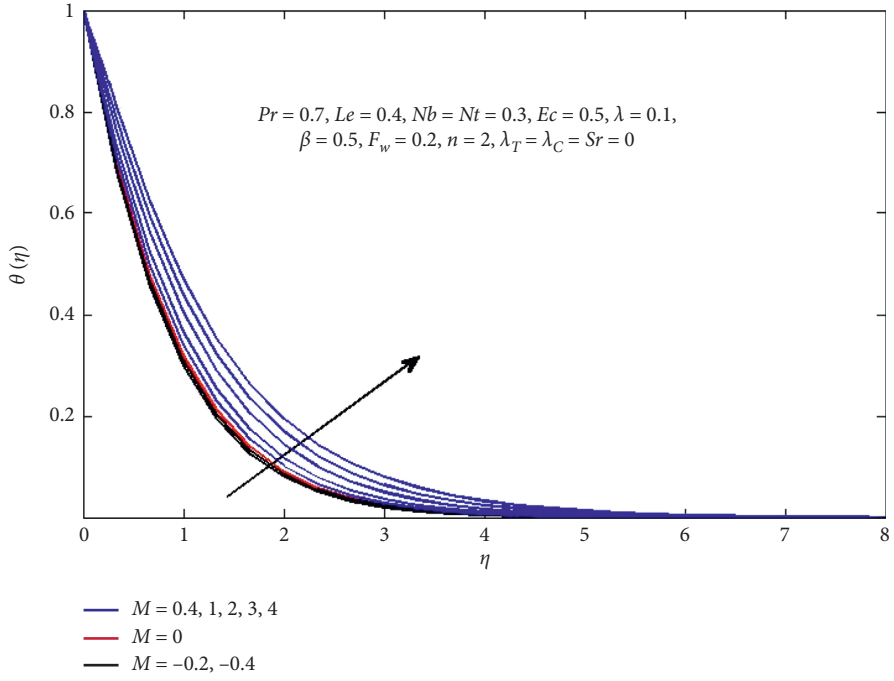

Figure 12: Variation of temperature θ concerning η with various values of M.

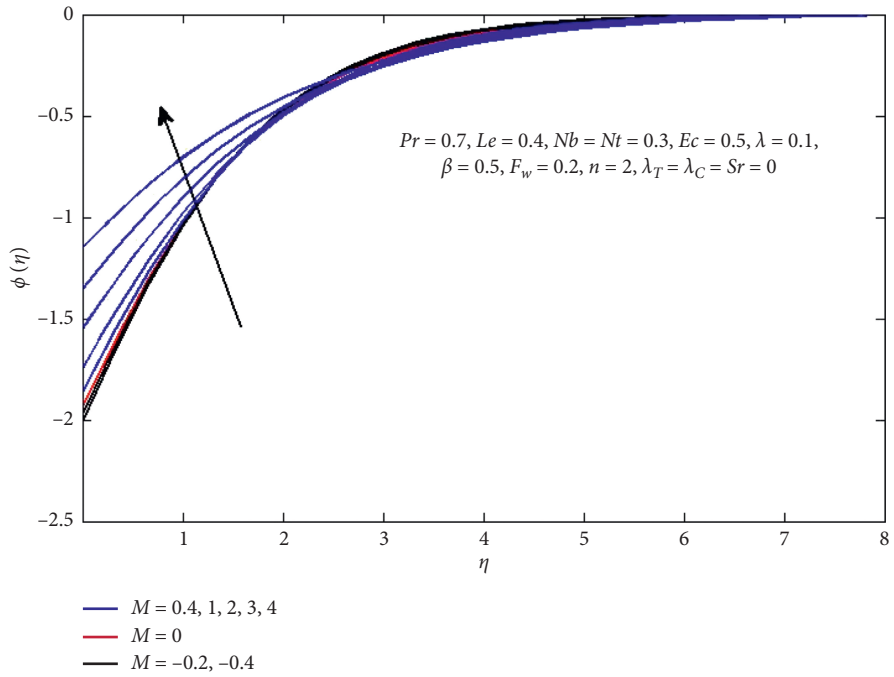

Figure 13: Variation of concentration ϕ concerning η with various values of M.

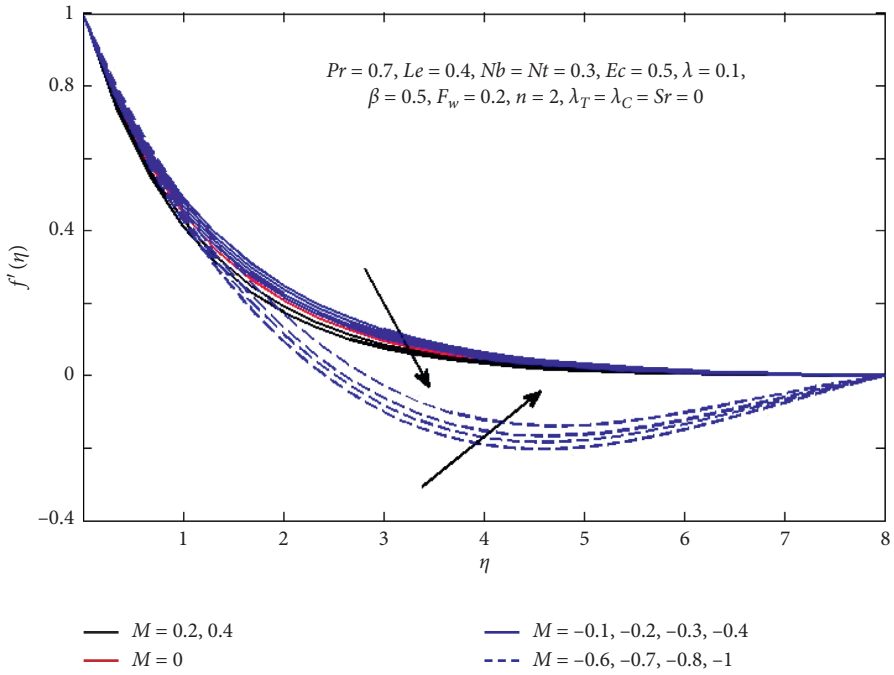

Figure 14: Variation of velocity f' concerning η with various values of M.

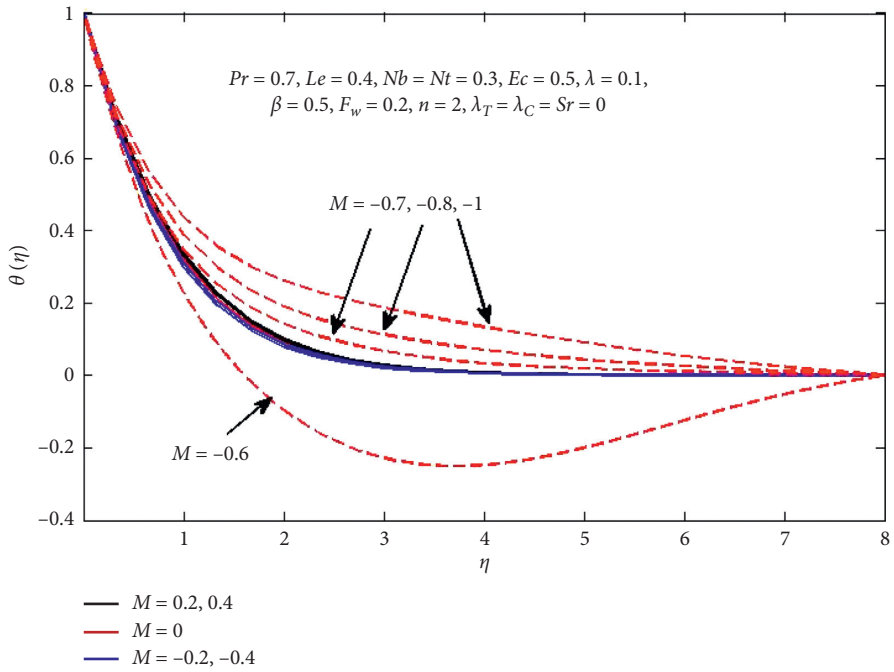

Figure 15: Variation of temperature θ concerning η with various values of M.

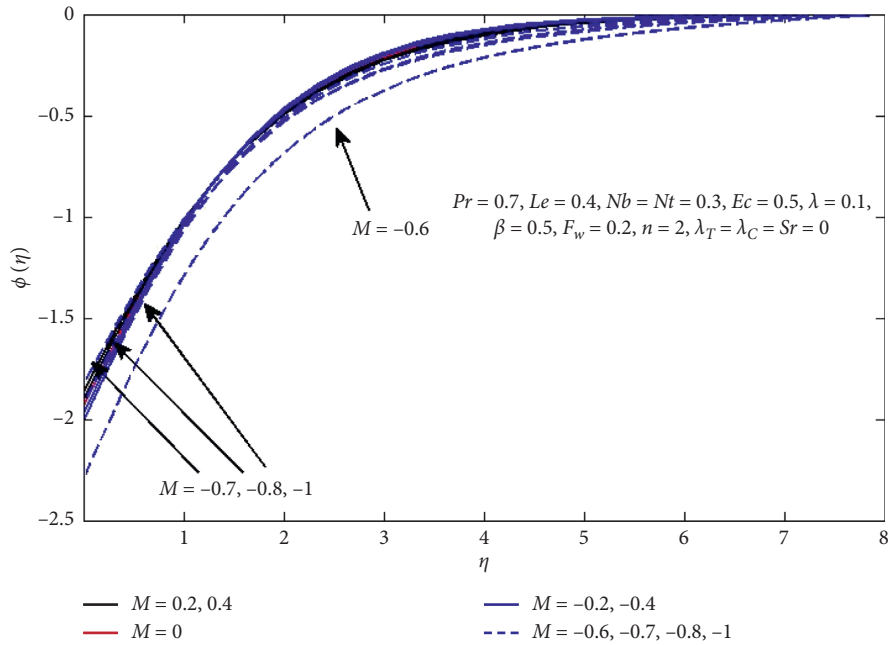

Figure 16: Variation of concentration ϕ concerning η with various values of M.

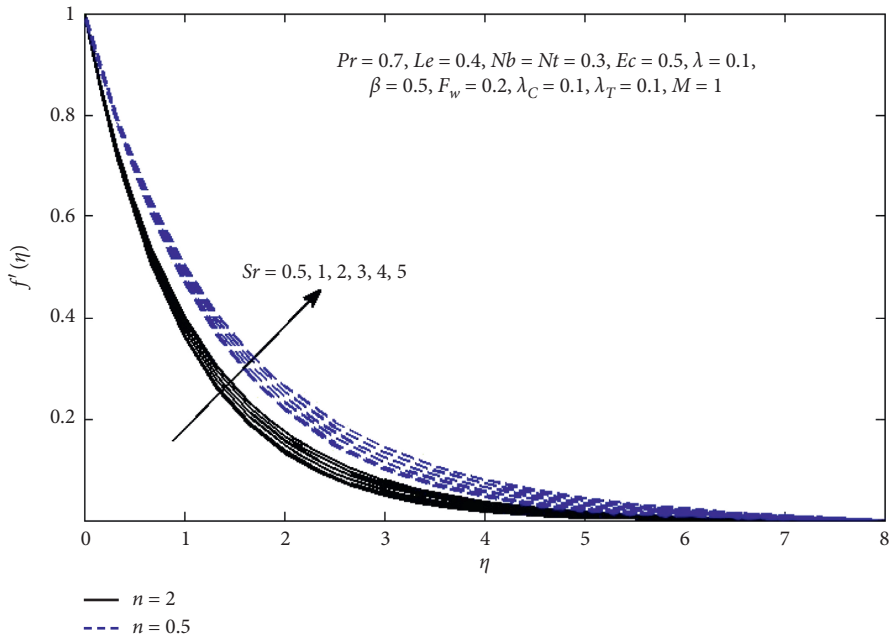

Figure 17: Variation of velocity f' concerning η with various values of Sr ($n = 2$ __, $n = 0.5$ ---).

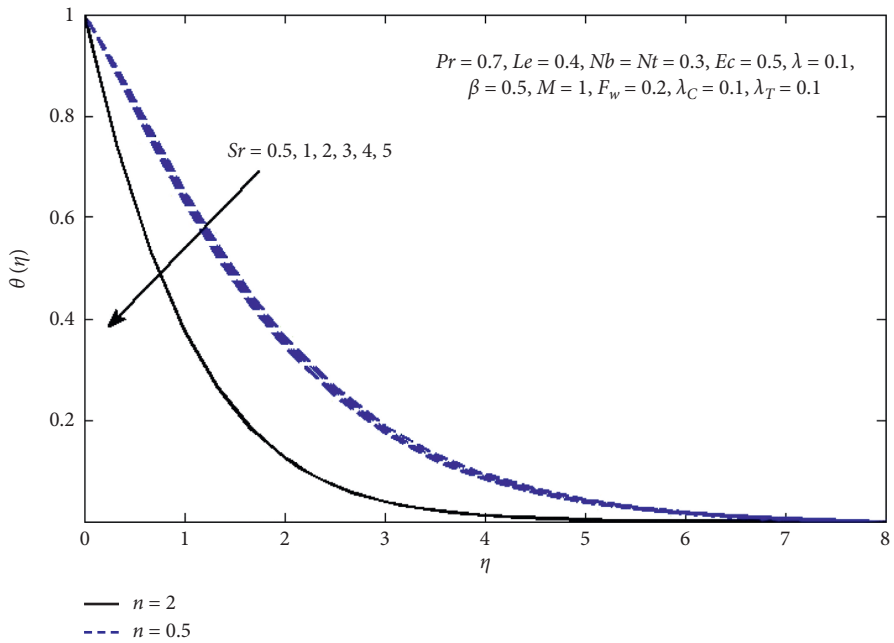

Figure 18: Variation of temperature θ concerning η with various values of Sr ($n = 2$ __, $n = 0.5$ ---).

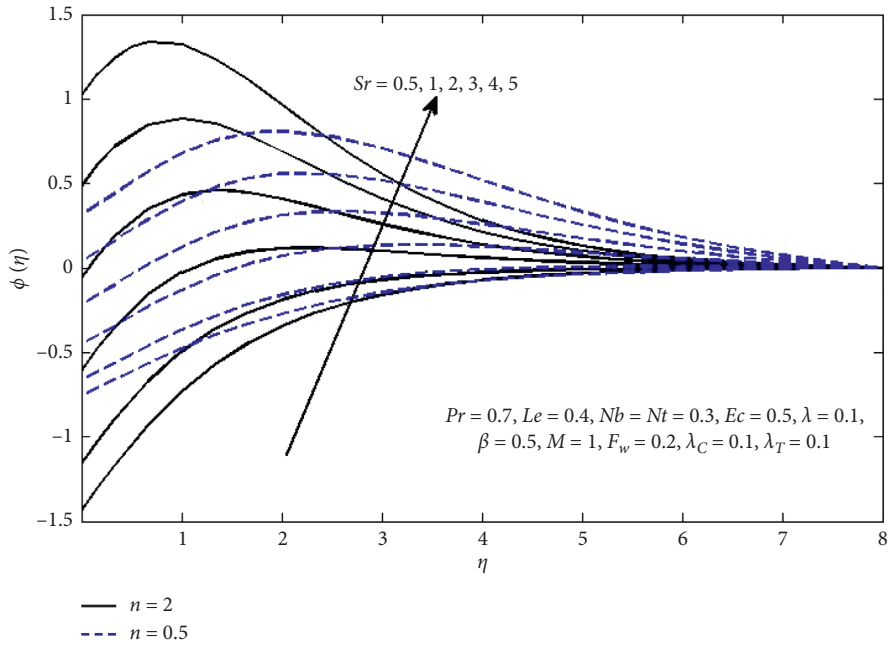

Figure 19: Variation of concentration ϕ concerning η with various values of Sr ($n = 2$ __, $n = 0.5$ ---).

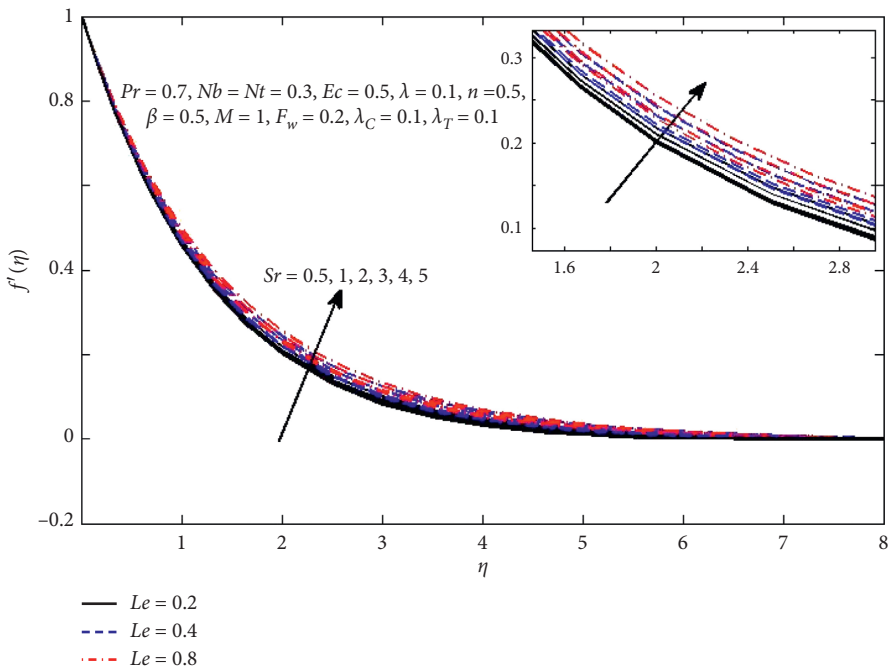

Figure 20: Variation of velocity f' concerning η with various values of Srand Le.

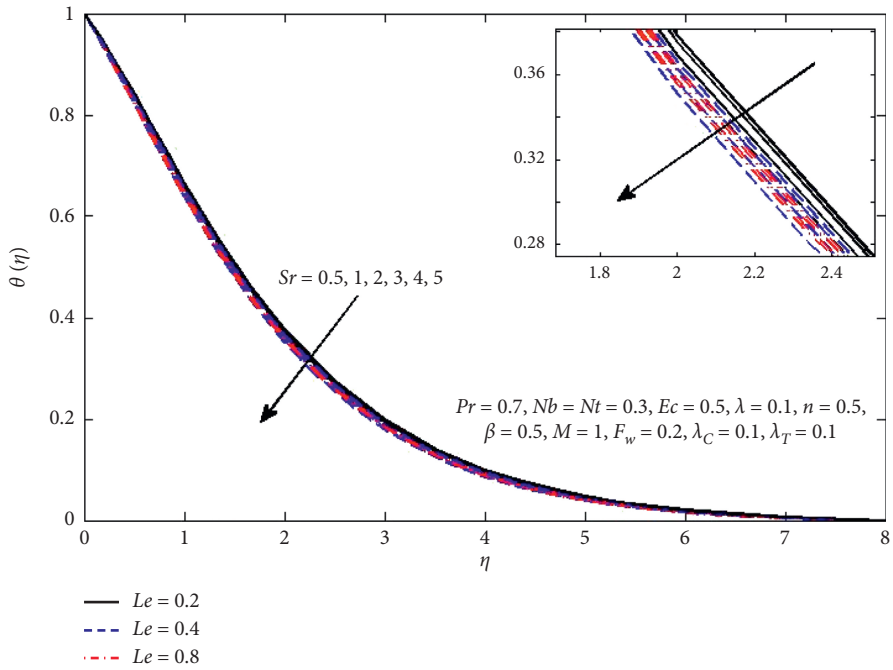

Figure 21: Variation of temperature θ concerning η with various values of Sr and Le.

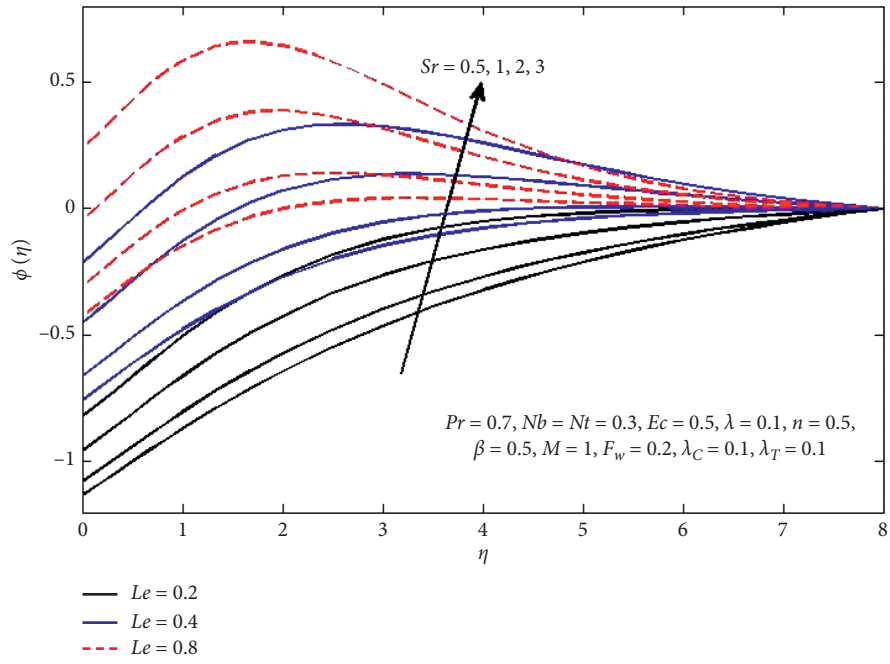

Figure 22: Variation of concentration ϕ concerning η with various values of Sr and Le.

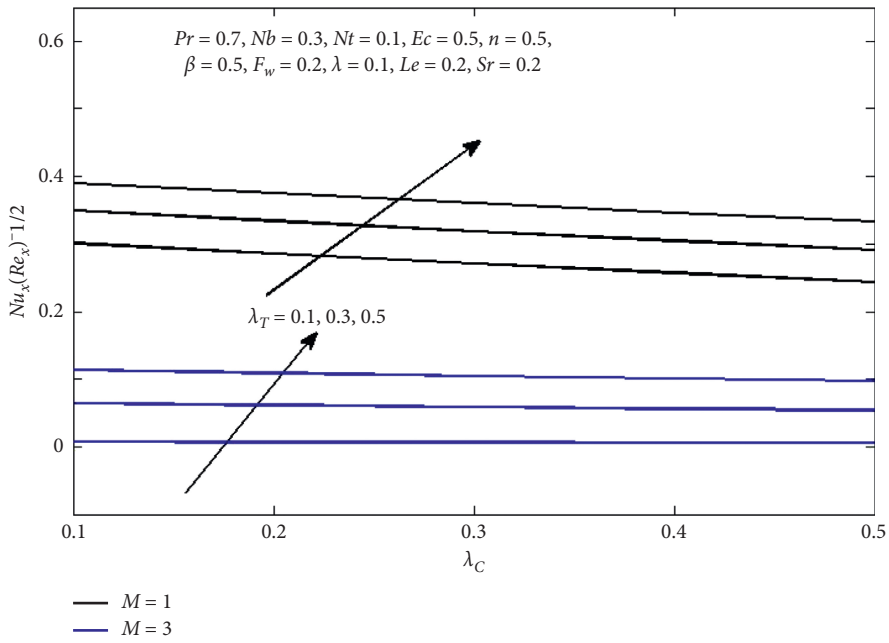

FIGURE 23: Variation of $\mathrm{Nu}_x\mathrm{Re}_x^{-1/2}$ concerning λ_c with various values of λ_T and M.

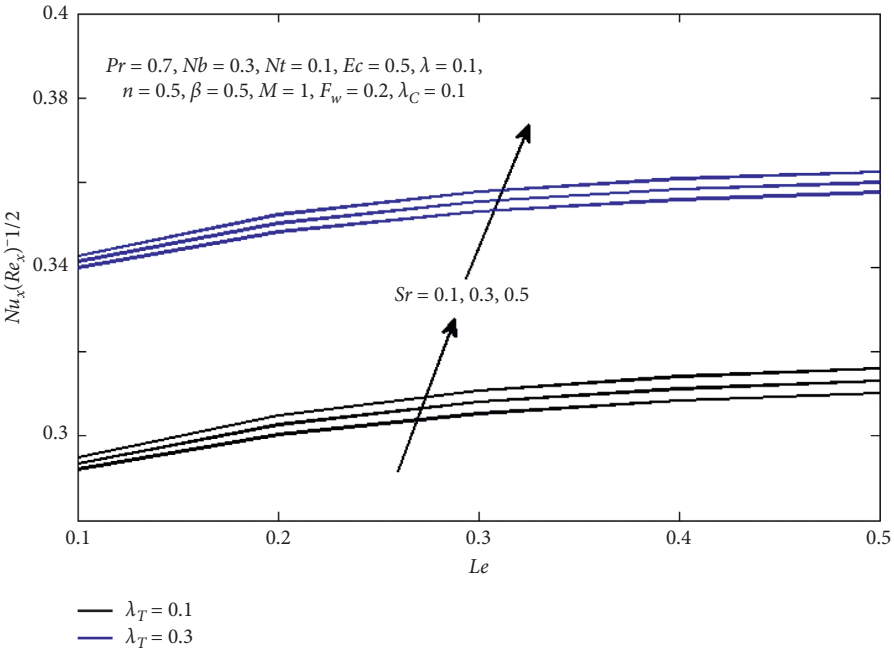

FIGURE 24: Variation of $\mathrm{Nu}_x\mathrm{Re}_x^{-1/2}$ concerning Lewith number various values of λ_T and Sr.

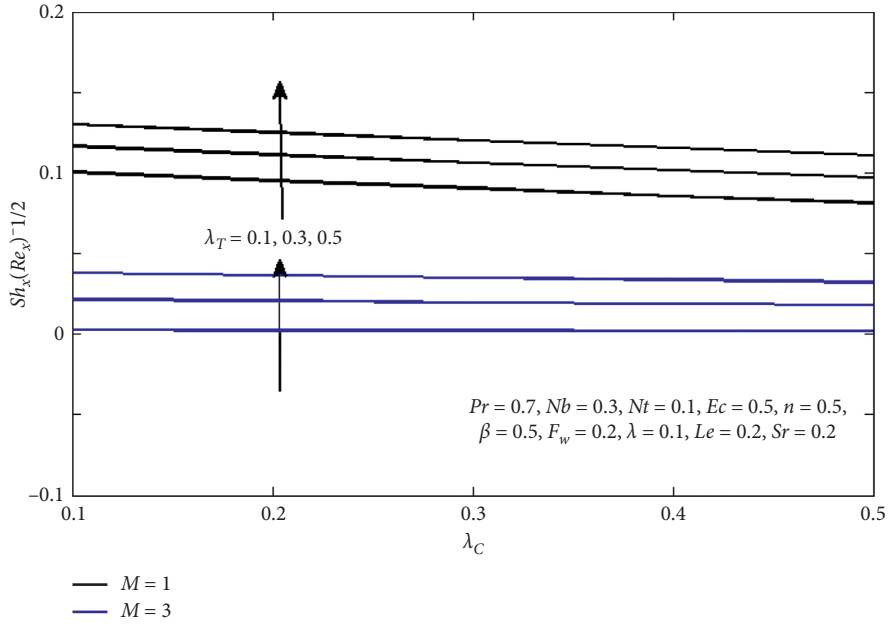

Figure 25: Variation of $\mathrm{Sh}_x\mathrm{Re}_x^{-1/2}$ concerning λ_T with various values of λ_c and M.

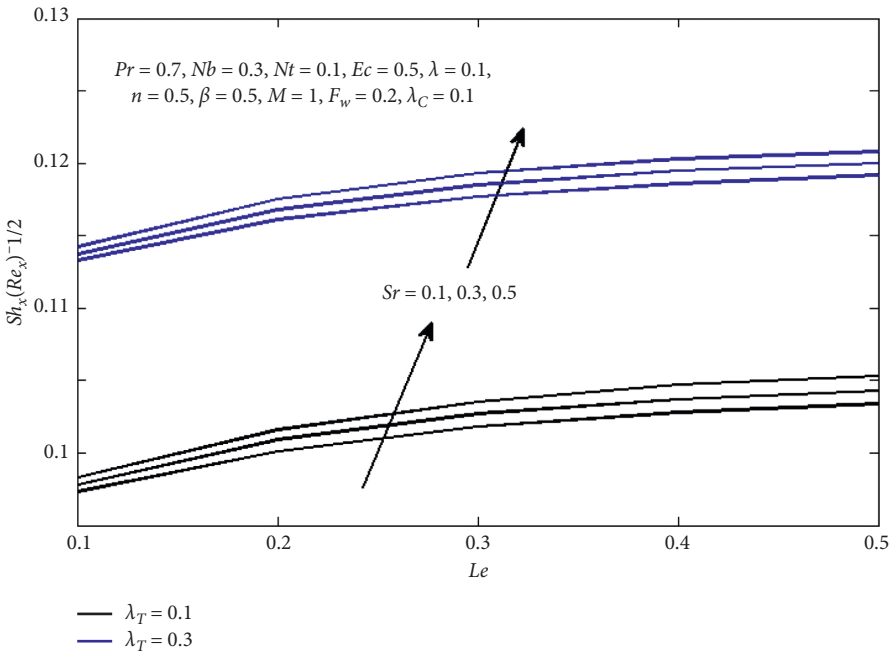

Figure 26: Variation of $\mathrm{Sh}_x\mathrm{Re}_x^{-1/2}$ concerning Lewith various values of λ_T and Sr.

4. Conclusion

In this research, the authors analyzed the impact of magnetic field M, Soret number Sr, heat source λ, thermal buoyancy parameter λ_T, and solutal buoyancy parameter λ_C of a nanofluid flow over convectively nonlinear heated due to an extending surface. The partial differential equations that dominate flow are transformed into normal changed-in-variables equations using the similarity transform and then solved numerically. The impacts of nondimensional ruling parameters specifically the Soret number of nanoparticles, magnetic field parameter, thermal buoyancy parameter λ_T, Lewith number, and λ_C on the flow, speed, temperature, and concentration profiles are discussed and presented graphically. The conclusions can be drawn as follows:

(1) The distribution of nanoparticle concentration is an increasing and decreasing function of the magnetic field and Soret number.

(2) Speed distribution decreases by increasing the values of the Soret number with growing values of the magnetic field.

(3) Temperature and concentration decrease with the increase of the values of thermal buoyancy parameter λ_T and solutal buoyancy parameter λ_C.

(4) Nusselt and Sherwood local numbers are greater for the incremental values of Soret number Sr and solutal buoyancy parameter λ_C.

For future work, we can use other influences of a nanofluid flow over convectively heated nonlinear due to an extending surface.

Data Availability

The data used to support the findings of this study are available from the corresponding author upon request.

Conflicts of Interest

The authors state that there are no conflicts of interest to report concerning the present study.

Authors' Contributions

All the authors contributed equally to this work.

Acknowledgments

The authors would like to acknowledge the financial support provided by the researchers of Taif University (TURSP-2020/162), Taif University, Taif, Saudi Arabia.

References

[1] C. Sulochana, M. K. K. Kumar, and N. Sandeep, "Process Engineering is at work during all stages of a continuous manufacturing process," *Chemical and Process Engineering Research*, vol. 37, p. 225, 2015.

[2] M. Wahiduzzaman, M. M. Miah, M. B. Hosssain, F. Johora, and S. Mistri, "Soret effect on mixed convection flow," *Dynamic Chaos*, vol. 2, p. 61, 2014.

[3] C. Ramreddy, P. V. S. N. Murthy, A. J. Chamkha, and A. M. Rashad, "Soret effect on mixed convection flow in a nanofluid under convective boundary condition," *International Journal of Heat and Mass Transfer International Journal of Heat and Mass Transfer*, vol. 64, pp. 384–392, 2013.

[4] C. S. K. Raju, M. J. Babu, N. Sandeep, V. Sugunamma, and J. V. Ramana Reddy, "Soret effect on mixed convection flow in a nanofluid under convective boundary condition," *Chemical and Process Engineering Research*, vol. 30, 2015.

[5] M. Ramzan, M. Bilal, J. D. Farooq, and U. Farooqd, "Mixed convective flow of Maxwell nanofluid past a porous vertical stretched surface-an optimal solution," *Results in Physics*, vol. 6, pp. 1072–1079, 2016.

[6] K.-L. Hsiao, "Stagnation electrical MHD nanofluid mixed convection with slip boundary on a stretching sheet," *Applied Thermal Engineering*, vol. 98, pp. 850–861, 2016.

[7] I. Ullah, I. Khan, and S. Shafie, "Stagnation electrical MHD nanofluid mixed convection with slip boundary on a stretching sheet," *Nanoscale Research Letters*, vol. 11, p. 527, 2016.

[8] M. P. Mkhatshwa, S. S. Motsa, M. S. Ayano, and P. Sibanda, "MHD mixed convective nanofluid flow about a vertical slender cylinder using overlapping multi-domain spectral collocation approach," *Case Studies in Thermal Engineering*, vol. 18, p. 100598, 2020.

[9] C.-J. Huang, "Influence of non-Darcy and MHD on free convection of non-Newtonian fluids over a vertical permeable plate in a porous medium with soret/dufour effects and thermal radiation," *International Journal of Thermal Sciences*, vol. 130, pp. 256–263, 2018.

[10] B. Mahanthesh and B. J. Gireesha, "Nonlinear radiative heat transfer in MHD three-dimensional flow of water based nanofluid over a non-linearly stretching sheet with convective boundary condition," *Journal of the Nigerian Mathematical Society*, vol. 35, no. 1, pp. 178–198, 2016.

[11] C. Gorla, *A Sheremet International Journal of Mechanical Sciences*, vol. 149, p. 26, 2018.

[12] J. M. N. Abad, R. Alizadeh, A. Fattahi, M. H. Doranehgard, and N. Karimi, "Nanofluid and porous fins effect on natural convection and entropy generation of flow inside a cavity," *Journal of Molecular Liquids*, vol. 23, Article ID 13492, 2020.

[13] M. Siavashi, R. Yousofvand, and S. Rezanejad, "Nanofluid and porous fins effect on natural convection and entropy generation of flow inside a cavity," *Advanced Powder Technology*, vol. 29, no. 1, pp. 142–156, 2018.

[14] M. Bilal, "Micropolar flow of EMHD nanofluid with nonlinear thermal radiation and slip effects," *Alexandria Engineering Journal*, vol. 59, no. 2, pp. 965–976, 2020.

[15] V. Kumar and S. V. S. S. N. V. G. Krishna Murthy, "Influence of MHD forces on Bejan's heatlines and masslines in a doubly stratified fluid saturated Darcy porous enclosure in the presence of Soret and Dufour effects-a numerical study," *International Journal of Heat and Mass Transfer*, vol. 117, pp. 1041–1062, 2018.

[16] A. S. Hashim and Hashim, "Heat transfer by natural convection of Fe3O4-water nanofluid in an annulus between a wavy circular cylinder and a rhombus," *International Journal of Heat and Mass Transfer*, vol. 130, pp. 320–332, 2019.

[17] K.-L. Hsiao, "Micropolar nanofluid flow with MHD and viscous dissipation effects towards a stretching sheet with multimedia feature," *International Journal of Heat and Mass Transfer*, vol. 112, pp. 983–990, 2017.

[18] S. Dinarv, R. Hosseini, M. Abulhasansari, and I. Pop, "Micropolar nanofluid flow with MHD and viscous dissipation effects towards a stretching sheet with multimedia feature," *Advanced Powder Technology*, vol. 26, no. 5, p. 1423, 2015.

[19] G. R. Kefayati and H. Tang, "MHD mixed convection of viscoplastic fluids in different aspect ratios of a lid-driven cavity using LBM," *International Journal of Heat and Mass Transfer*, vol. 124, pp. 344–367, 2018.

[20] M. Ramzan, M. Bilal, U. Farooq, and J. D. Chung, "Mixed convective radiative flow of second grade nanofluid with convective boundary conditions: an optimal solution," *Results in Physics*, vol. 6, pp. 796–804, 2016.

[21] V. Kumar, S. V. S. S. N. V. G. K. Murthy, and B. V. R. Kumar, "Bejan's heatline and massline visualization of multi-force effect on convection in a porous enclosure," *International Journal of Mechanical Sciences*, vol. 146-147, pp. 249–271, 2018.

[22] S. Aurangzaib K Bhattacharyya, K. Bhattacharyya, and S. Shafie, "Effect of partial slip on an unsteady MHD mixed

convection stagnation-point flow of a micropolar fluid towards a permeable shrinking sheet," *Alexandria Engineering Journal*, vol. 55, no. 2, pp. 1285–1293, 2016.

[23] M. V. Krishna and A. J. Chamkha, "Hall and ion slip effects on MHD rotating flow of elastico-viscous fluid through porous medium," *International Communications in Heat and Mass Transfer*, vol. 113, Article ID 104494, 2020.

[24] S. Z. A. Zaidi and S. T. Mohyud-Din, "Analysis of wall jet flow for Soret, Dufour and chemical reaction effects in the presence of MHD with uniform suction/injection," *Applied Thermal Engineering*, vol. 103, pp. 971–979, 2016.

[25] G. R. Machireddy and S. Naramgari, "Heat and mass transfer in radiative MHD Carreau fluid with cross diffusion," *Ain Shams Engineering Journal*, vol. 9, no. 4, pp. 1189–1204, 2018.

[26] A. I. Alsabery, M. A. Sheremet, M. Ghalambaz, A. J. Chamkha, and I. Hashim, "Fluid-structure interaction in natural convection heat transfer in an oblique cavity with a flexible oscillating fin and partial heating," *Applied Thermal Engineering*, vol. 145, pp. 80–97, 2018.

[27] M. Safaei and R. Bhargava, "Finite element solution of double-diffusive boundary layer flow of viscoelastic nanofluids over a stretching sheet," *Computational Mathematics and Mathematical Physics*, vol. 54, no. 5, pp. 848–863, 2014.

[28] Y. Do, G. K. Ramesh, G. S. Roopa, and M. Sankar, "Double-diffusive radiative magnetic mixed convective slip flow with Biot and Richardson number effects," *Journal of Central South University*, vol. 26, p. 2000, 2019.

[29] O. A. Bég, M. J. Uddin, M. M. Rashidi, and N. Kavyani, "Double-diffusive radiative magnetic mixed convective slip flow with Biot and Richardson number effects," *Journal of Engineering Thermophysics*, vol. 23, no. 2, pp. 79–97, 2014.

[30] D. Srinivasacharya and P. Jagadeeshwar, "Slip viscous flow over an exponentially stretching porous sheet with thermal convective boundary conditions," *International Journal of Applied and Computational Mathematics*, vol. 3, no. 4, pp. 3525–3537, 2017.

[31] A. Chemi, H. Heireche, and M. Zidour, K. Rakrak and A. A. Bousahla, "Critical buckling load of chiral double-walled carbon nanotube using non-local theory elasticity," *Advances in Nano Research*, vol. 3, no. 4, pp. 193–206, 2015.

[32] A. Chemi, "Advances in Nano research," *International Journal*, vol. 9, no. 2, p. 69, 2020.

[33] S. S. Mirjavadi, M. Nikookar, S. Mollaee, M. Forsat, M. R. Barati, and A. M. S. Hamouda, "Advances in nano research," *International Journal*, vol. 9, no. 1, pp. 47–58, 2020.

[34] S. M. Abo-Dahab, M. A. Abdelhafez, F. Mebarek-Oudina, and S. M. Bilal, "Advances in nano research," *Indian Journal of Physics*, vol. 2020, 2020.

[35] K. Rafique, M. I. Anwar, M. Misiran et al., "Stagnation electrical MHD nanofluid mixed convection with slip boundary on a stretching sheet," *Frontiers Physics*, vol. 23, Article ID 00139, 2019.

[36] O. R. Alomar, N. M. Basher, and A. A. Yousif, "Analysis of effects of thermal non-equilibrium and non-Darcy flow on natural convection in a square porous enclosure provided with a heated L shape plate," *International Journal of Mechanical Sciences*, vol. 181, p. 105704, 2020.

[37] H. Maleki, J. Alsarraf, A. Moghanizadeh, and H. Hajabdollahi, "Heat transfer and nanofluid flow over a porous plate with radiation and slip boundary conditions," *Journal of Central South University*, vol. 26, no. 5, pp. 1099–1115, 2019.

[38] H. Singh, "Advances in nano research," *Nonlinear Science Letter A*, vol. 8, no. 4, pp. 397–404, 2017.

[39] H. Singh, "Advances in nano research," *International Journal of Applied and Computational Mathematics*, vol. 3, no. 4, pp. 3705–3722, 2017.

[40] H. Singh and H. M. Srivastavabc, "Advances in nano research," *Physica A*, vol. 523, pp. 1130–1149, 2019.

[41] H. Singh, "Advances in nano research," *Chaos Solitons & Fractals*, vol. 138, 2020.

[42] H. Singh, "Numerical Methods for Partial Differential Equations," 2020.

[43] H. Singh, "International Journal of Dynamic and Control," 2020.

[44] M. Hussain, M. N. Naeem, A. Tounsi, and M. Taj, "Advances in nano research," *Advances in Nano Research*, vol. 7, no. 6, pp. 431–442, 2019.